Polymer Acid Doped Polyaniline Is Electrochemically Stable Beyond pH 9

Jacob Tarver,[†] Joung Eun Yoo,[†,‡] T. Joseph Dennes,[§] Jeffrey Schwartz,[§] and Yueh-Lin Loo*,[†]

Department of Chemical Engineering and Department of Chemistry, Princeton University, Princeton, New Jersey 08544 and Department of Chemical Engineering, University of Texas at Austin, Austin, Texas 78712

Received August 27, 2008

We report the pH dependence of the electrochemical redox behavior of polyaniline (PANI) that is template synthesized with poly(2-acrylamido-2-methyl-1-propanesulfonic acid), PAAMPSA. Cyclic voltammetry and spectroelectrochemistry were used to assess the oxidation and protonation states of PANI−PAAMPSA. Stable and reversible pernigraniline−emeraldine−leucoemeraldine transitions extend beyond pH 7. Direct pernigraniline−leucoemeraldine transitions dominate in alkaline conditions; these transitions are stable and reversible between 7 and 10, extending the pH stability of PANI well beyond those previously reported.

Introduction

Polyaniline (PANI) has long been considered a strong contender in the field of polymer electronics due to its varied electrochromic effects[1] and the unique origin of its conductive form.[2] Unlike many other conductive polymers, such as polyacetylene[3,4] and polythiophene,[5,6] PANI relies on a nonredox protonic doping mechanism and is inherently more resilient to the oxidizing environment presented in ambient conditions.[7] In its fully oxidized and reduced states (see Scheme 1a and 1c) PANI is electrically insulating and referred to as pernigraniline base (PB) and leucoemeraldine base (LB), respectively. An intermediate oxidation state containing an equal number of oxidized and reduced repeat units exists between these two extremes (Scheme 1b) and is referred to as emeraldine base (EB). Electrically conductive emeraldine salt (ES) results from exposing EB to a proton source (Scheme 1d).[8] The diverse and flexible chemistry of PANI has led to much effort toward incorporating PANI into organic-based electronic,[9,10] electrochromic,[11] and sensing devices.[12] Early studies using small-molecule proton sources, such as hydrochloric acid[13] and camphorsulfonic acid,[14,15] reported conductivities spanning 10−300 $S \cdot cm^{-1}$ but cited negligible solubility and diminished electrochemical redox behavior above pH 4[16] due to neutralization and subsequent dopant diffusion when ES is converted to EB. The volatile nature of these small-molecule acids also led to diminished conductivities upon long-term storage, compromising the stability attributed to the nonredox doping mechanism.

Several methods have been proposed to solubilize ES while retaining electroactivity (i.e., redox behavior) at elevated pH. Sulfonating the benzenoid rings to produce self-doped PANI obviates issues of dopant volatility and diffusivity while widening the electroactive range toward alkaline conditions.[17,18] This derivatization of PANI also imparts practical levels of solubility to the final product.[19] The sulfonation reaction, however, can hydrolyze PANI;[20] the electrical conductivity of the resulting polymer is generally reduced as a consequence ($\leq 10^{-1}$ $S \cdot cm^{-1}$).[21] As such, use of polyanions, such as poly(acrylic acid),[22] poly(styrene sulfonate),[23,24] and poly(2-acrylamido-2-methyl-1-propanesulfonic acid) (PAAMPSA),[25,26] as dopants has been actively

* To whom correspondence should be addressed. E-mail: lloo@princeton.edu.
† Department of Chemical Engineering, Princeton University.
‡ Department of Chemical Engineering, University of Texas at Austin.
§ Department of Chemistry, Princeton University.

(1) Trevedi, D. C. In *Conductive Polymers: Synthesis and Electrical Properties, Handbook of Organic Conductive Molecules and Polymers*; Nalwa H. S., Ed.; Wiley: New York, 1997; Vol. 2.
(2) Chiang, J.-C.; MacDiarmid, A. G. *Synth. Met.* **1986**, *13*, 193.
(3) Chiang, C. K.; Fincher, C. R., Jr.; Park, Y. W.; Heeger, A. J.; Shirakawa, H.; Louis, E. J.; Gau, S. C.; MacDiarmid, A. G. *Phys. Rev. Lett.* **1977**, *39*, 1098.
(4) Chiang, C. K.; Park, Y. W.; Heeger, A. J. *J. Chem. Phys.* **1978**, *69*, 5098.
(5) Schopf, G.; Koβmehl, G. *Adv. Polym. Sci.* **1997**, *129*, 1.
(6) Loponen, M. T.; Taka, T.; Laakso, J.; Väkiparta, K.; Suuronen, K.; Valkeinen, P.; Österholm, J. E. *Synth. Met.* **1991**, *41*, 479.
(7) Wnek, G. E. *Synth. Met.* **1986**, *15*, 213.
(8) Heeger, A. J. *Rev. Mod. Phys.* **2001**, *73*, 681.
(9) Lee, K. S.; Blanchet, G. B.; Gao, F.; Loo, Y.-L. *Appl. Phys. Lett.* **2005**, *86*, 074102.
(10) Lee, K. S.; Smith, T. J.; Dickey, K. C.; Yoo, J. E.; Stevenson, K. J.; Loo, Y.-L. *Adv. Funct. Mater.* **2006**, *16*, 2409.
(11) Kobayashi, T.; Yoneyama, H.; Tamura, H. *J. Electroanal. Chem.* **1984**, *161*, 419.
(12) Zhang, L.; Dong, S. *J. Electroanal. Chem.* **2004**, *568*, 189.
(13) MacDiarmid, A. G.; Chiang, J.-C.; Halpern, M.; Huang, W.-S.; Mu, S.-L.; Somasiri, N. L. D.; Wu, W.; Yaniger, S. I. *Mol. Cryst. Liq. Cryst.* **1985**, *121*, 173.
(14) MacDiarmid, A. G.; Epstein, A. J. *Synth. Met.* **1995**, *69*, 85.
(15) Avylanov, J. K.; Min, Y.; MacDiarmid, A. G.; Epstein, A. J. *Synth. Met.* **1995**, *72*, 65.
(16) Diaz, A. F.; Logan, J. A. *J. Electroanal. Chem.* **1980**, *111*, 111.
(17) Lukachova, L. V.; Shkerin, E. A.; Puganova, E. A.; Karyakaina, E. E.; Kiseleva, S. G.; Orlov, A. V.; Karpacheva, G. P.; Karyakin, A. A. *J. Electroanal. Chem.* **2003**, *544*, 59.
(18) Li, C.; Mu, S. *Synth. Met.* **2005**, *149*, 143.
(19) Yue, J.; Epstein, A. J.; MacDiarmid, A. G. *Mol. Cryst. Liq. Cryst.* **1990**, *189*, 255.
(20) Wei, X.; Epstein, A. J. *Synth. Met.* **1995**, *74*, 123.
(21) Yue, J. *J. Am. Chem. Soc.* **1990**, *112*, 2800.
(22) Hwang, J. H.; Yang, S. C. *Synth. Met.* **1989**, *29*, E271.

10.1021/cm802314h CCC: $40.75
Published on Web 12/19/2008

Scheme 1. Vertical Reaction Sequence Shows Redox Transitions between (a) PB, (b) EB, and (c) LB; Horizontal Reaction Sequence Demonstrates Proton Doping of EB to (d) ES[a]

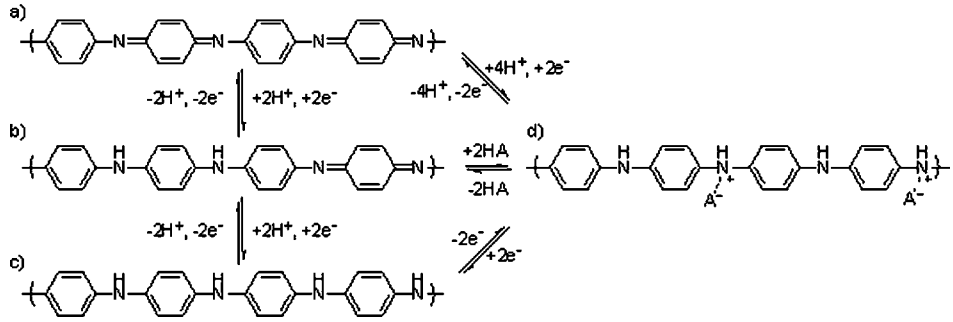

[a] A^- represents counterion from the proton source.

investigated as an alternative to producing solution-processable PANI. Polymer acids offer many advantages over conventional small-molecule acid dopants. In particular, because not all acid groups along the polymer chain participate in the doping process, excess acid groups render water dispersibility to the conductive form of PANI.[27] Use of such high molecular weight dopants also improves morphological control,[22,28] eliminates dopant volatility and diffusivity, and extends the electroactivity of the final polymer beyond pH 4.[22] Until recently, polymer acid doped PANI systems, like self-doped PANI, have generally struggled to achieve conductivities greater than 10^{-1} S·cm^{-1}.[29−31]

Research within our group has established oxidative template polymerization of aniline on PAAMPSA as a promising method of conferring water solubility while maintaining conductivities (0.4−2.4 S·cm^{-1}) exceeding those of any previously described template-polymerized PANI system.[32,33] PAAMPSA has amide groups that can hydrogen bond; we thus attribute this conductivity enhancement to the structure of the polymer complex that is formed due to specific interactions between PANI and PAAMPSA.[32] It follows that PANI−PAAMPSA forms an efficient redox couple for glucose sensing at physiological pH (7.2), yielding unprecedented current densities (225 μA·cm^{-2}).[34] Here, we report the pH dependence of the oxidation/dopant states of PANI−PAAMPSA. Our studies indicate that the electroactivity of PANI−PAAMPSA is stable and reversible in excess of pH 9. In fact, electrochemical redox transitions are observed as high as pH 10.2. A gradual loss of activity, however, occurs at this pH upon prolonged immersion (>40 min). Compared to PANI that is doped with small-molecule acids, PANI−PAAMPSA exhibits unprecedented electroactivity over 8 decades of pH. We attribute this unusual electrochemical stability of PANI−PAAMPSA to the same specific interactions that are responsible for the enhanced conductivity observed in the solid state of these materials.

Experimental Section

Aniline (Fisher Scientific, 99.9%), ammonium peroxydisulfate (98.9%, Fisher Scientific), and poly(2-acrylamido-2-methyl-1-propanesulfonic acid) (PAAMPSA, 10.36 wt % in water, reported M_w = 800 kg·mol^{-1}, Scientific Polymer Products) were used as purchased. PANI was template synthesized on PAAMPSA per previous reports by Yoo et al.[32,33] Aniline monomer was mixed with PAAMPSA at a 1:1 monomer to acid molar ratio in deionized water. Ammonium peroxydisulfate was then added to the mixture dropwise at a 1:0.9 monomer to oxidizing agent molar ratio. Polymerization was carried out at 70 mM while immersed in an ice bath for 24 h. Acetone was slowly added to precipitate the resulting PANI−PAAMPSA complex. After cleanup and drying under dynamic vacuum, PANI−PAAMPSA was stirred at 5 wt % in water for at least 10 days before use to ensure complete dispersion. Electrochemical studies in pH 3−6 were performed in acetate buffer solutions (ABS) containing sodium acetate (anhydrous, 99.0%, EMD Chemicals) and acetic acid (glacial, 100.0%, Fisher Scientific); studies across pH 7−9 were performed in phosphate buffer solutions (PBS) containing sodium phosphate monobasic monohydrate (99.6%, Fisher Scientific) and sodium phosphate dibasic heptahydrate (98.9%, Fisher Scientific). Carbonate buffers containing sodium carbonate (anhydrous, 99.5%, EMD Chemicals) and sodium bicarbonate (99.7%, EMD Chemicals) were used to assess the electroactivity of PANI−PAAMPSA at pH 10−11. Buffer pH was measured using an Orion 210A+ pH meter. Water was deionized to 18.2 MΩ prior to buffer preparation using a Milli-Q Academic purification system.

Cyclic voltammetry (CH-Instruments CHI-660 electrochemical workstation, CHI-200 Faraday cage) was performed in a one-compartment cell to study the electroactivity of PANI−PAAMPSA films on glassy-carbon (GC) working electrodes. Platinum-wire counter electrodes and silver/silver chloride reference electrodes were purchased from CH-Instruments. Silver/silver chloride (Ag/AgCl) reference electrodes were stored in 3.0 M potassium chloride (99.0%, EMD) solutions when not in use. GC electrodes were purchased from CH-Instruments and polished using a sequence of 15, 3, and 1 μm diamond grit suspensions (Bioanalytical Services) prior to PANI−PAAMPSA deposition at 60 μg·cm^{-2} loading. After deposition, the electrodes were allowed to dry in ambient conditions

(23) Kang, Y.; Lee, M.-H.; Rhee, S. B. *Synth. Met.* **1992**, *52*, 319.
(24) Hyodo, K.; Omae, M.; Kagami, Y. *Electrochim. Acta* **1991**, *36*, 357.
(25) Lapkowski, M. *Synth. Met.* **1993**, *55*, 1558.
(26) Ivanov, V. F.; Gribkova, O. L.; Cheberyako, K. V.; Nekrasov, A. A.; Tverskoi, V. A.; Vannikov, A. V. *Russ. J. Electrochem.* **2004**, *40*, 299.
(27) Angelopoulos, M.; Patel, N.; Shaw, J. M.; Labianca, N. C.; Rishton, S. A. *J. Vac. Sci. Technol. B* **1993**, *11*, 2794.
(28) Bucholz, T. L.; Loo, Y.-L. *Macromolecules* **2008**, *41*, 4069.
(29) Chen, S.-A.; Lee, H.-T. *Macromolecules* **1995**, *28*, 2858.
(30) Moon, H.-S.; Park, J.-K. *Synth. Met.* **1998**, *92*, 223.
(31) Cai, L. T.; Chen, H. Y. *J. Appl. Electrochem.* **1998**, *28*, 161.
(32) Yoo, J. E.; Cross, J. L.; Bucholz, T. L.; Lee, K. S.; Espe, M. P.; Loo, Y.-L. *J. Mater. Chem.* **2007**, *17*, 1268.
(33) Yoo, J. E.; Bucholz, T. L.; Jung, S.; Loo, Y.-L. *J. Mater. Chem.* **2008**, *18*, 3129.
(34) Mano, N.; Yoo, J. E.; Tarver, J.; Loo, Y.-L.; Heller, A. *J. Am. Chem. Soc.* **2007**, *129*, 7006.

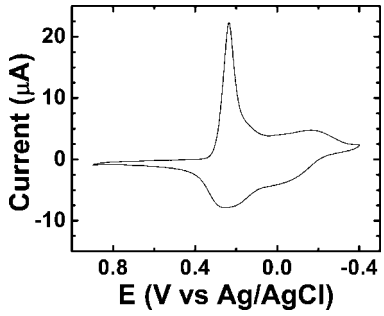

Figure 1. Cyclic voltammogram of PANI−PAAMPSA loaded at 60 $\mu g \cdot cm^{-2}$ on a glassy-carbon electrode and immersed in a 100 mM pH 5 acetate buffer solution. Tenth cycle shown at a scan rate of 20 $mV \cdot s^{-1}$. The primary redox couple centered at 0.23 V corresponds to the PB to emeraldine reaction, while the secondary couple centered at −0.1 V is associated with the emeraldine to LB transition.

for more than 2 h before use. Electroactivity was assessed over a −0.4 to +0.9 V (vs Ag/AgCl) potential window at a constant sweep rate of 20 $mV \cdot s^{-1}$.

Spectral characterization was performed on PANI−PAAMPSA spin coated on indium tin oxide ((ITO; 15 $\Omega \cdot square^{-1}$, Colorado Concept Coatings) coated glass substrates in the UV−vis/NIR range from 280 to 1100 nm using an Agilent 8453 spectrophotometer with 1 nm resolution. To eliminate complexities arising from film delamination during spectral measurements, a monolayer of (12-phosphonododecyl)phosphonic acid (bisphosphonic acid, 97%, Aldrich) was covalently bound to the ITO to promote PANI−PAAMPSA adhesion using the tethering by aggregation and growth (T-BAG) deposition method developed by Schwartz et al.[35] Monolayer deposition was performed using a 95 vol % tetrahydrofuran (THF, distilled in-house to ensure anhydrous and inhibitor-free conditions)/5 vol % methyl alcohol (anhydrous, 99.8%, Acros) solution containing 0.1 mM bisphosphonic acid. ITO substrates were suspended within the solution. As the solution was drawn down by evaporation, the bisphosphonic acid deposited on the substrates at the air/liquid interface. Substrates were then baked for 24 h at 130 °C post-evaporation to drive the condensation reaction between the phosphonic acid groups and the oxide surface on the ITO to completion. The phosphonic-acid-modified ITO was sonicated for 10 min in ethanol (100%, Pharmaco-Aaper) and dried under nitrogen prior to spin coating a 5 wt % PANI−PAAMPSA aqueous dispersion at 5000 rpm. Spectral characterization of phosphonic-acid-modified ITO in the UV−visible region showed no deviations from pristine ITO; a clean ITO substrate was therefore used as background in subsequent measurements. Spectroelectrochemical measurements were performed using the spectrophotometer and electrochemical workstation in combination with a custom-designed spectroelectrochemical cell. Spectra were collected every 4 s to ensure a sufficient signal integration time.

Results and Discussion

Electroactivity Assessment of PANI−PAAMPSA-Modified Glassy-Carbon Electrodes. Figure 1 shows a cyclic voltammogram (CV) of a PANI−PAAMPSA-modified glassy carbon electrode in 100 mM, pH 5.0 phosphate buffer solution measured at a 20 $mV \cdot s^{-1}$. Two redox couples are observed at 0.23 and −0.10 V (vs Ag/AgCl) and are henceforth referred to as the primary and secondary couples, respectively. The reduction (positive current) and oxidation (negative current) peaks for the primary couple are separated by only 48 mV, indicating a high degree of reversibility. The redox peaks associated with the secondary couple are separated by nearly 150 mV. Large peak separation for this secondary couple has previously been observed in HCl-doped PANI systems and is attributed to slow charge-transfer kinetics.[36] Though the large overpotential suggests hindered reversibility, repeated cycling does not lead to current losses or shifts in peak potentials. We therefore deem the multistep reaction as a whole to be stable and reversible over the time scales examined (hundreds of cycles exceeding 10 h of continuous immersion).

At the oxidizing extreme of Figure 1 PANI exists in the PB state while LB dominates at the reducing extreme. PANI thus transitions from the PB state to the emeraldine form upon traversing the primary redox couple on reduction before converting to LB at the reducing extreme and from LB to the emeraldine form upon traversing the secondary redox couple on oxidation. It is, however, not immediately clear from cyclic voltammetry whether the intermediate emeraldine state that is accessed on reduction of PB and oxidation of LB is in the base or salt form of PANI as EB and ES share the same electronic environment. Given that EB and ES have the same number of electrons they are indistinguishable via potentiometric methods alone. However, EB and ES forms of PANI do differ in proton count; their presence can thus be distinguished by determining the pH dependence of the potentials of the redox couples. The pH dependence of a simple redox reaction, such as that illustrated in eq 1, can be predicted by the Nernst equation[37]

$$\mathrm{O} + n\mathrm{e}^- + m\mathrm{H}^+ \leftrightarrow \mathrm{R}$$

$$E = \left(E^0 + \frac{0.059}{n}\ln\frac{[\mathrm{O}]}{[\mathrm{R}]}\right) - 0.059\frac{m}{n}\mathrm{pH} \qquad (1)$$

where O and R represent the oxidized and reduced species, respectively, E and E^0 represent the actual and standard potentials, respectively, 0.059 represents the ratio of the gas constant to the Faraday constant at room temperature, n represents the number of reacting electrons, and m represents the number of reacting protons. [O] and [R] thus represent bulk concentrations of the oxidized and reduced species, respectively.

According to Scheme 1 transitions between PB and EB and those between EB and LB involve the exchange of two protons and two electrons. In accordance with eq 1, $m = n = 2$; the redox couples associated with these transitions would thus shift −59 mV/decade of pH. On the other hand, transitions between PB and ES involve four protons and two electrons. If the primary couple was associated with the transition from PB to ES and vice versa, one would expect a shift in potential of −118 mV/decade of pH instead ($m = 4$; $n = 2$). Since proton exchange does not take place during the transitions between ES and LB and in accordance with eq 1 for $m = 0$ the redox couple associated with this transition should be independent of pH.

(35) Hanson, E. L.; Schwartz, J.; Nickel, B.; Koch, N.; Danisman, M. F. *J. Am. Chem. Soc.* **2003**, *125*, 16074.
(36) Foot, P. J. S.; Simon, R. *J. Phys. D: Appl. Phys.* **1989**, *22*, 1598.
(37) Bard, A. J.; Faulkner, L. R. *Electrochemical Methods: Fundamentals and Applications*; Wiley: New York, 2001.

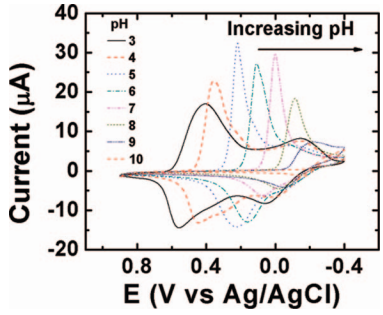

Figure 2. Cyclic voltammograms of PANI−PAAMPSA loaded at 60 $\mu g \cdot cm^{-2}$ on glassy-carbon electrodes and immersed in 100 mM buffer solutions of varying pH. Scan rate was held constant at 20 $mV \cdot s^{-1}$ over 10 cycles. Tenth cycles shown.

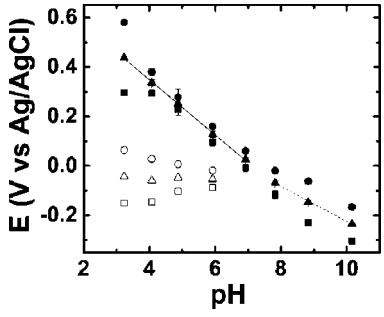

Figure 3. Oxidation (E_{ox}, ●), reduction (E_{red}, ■), and redox ($E_{1/2}$, ▲) potentials of PANI−PAAMPSA's primary couple as a function of pH. Oxidation (E_{ox}^2, ○), reduction (E_{red}^2, □), and redox potentials ($E_{1/2}^2$, Δ) of PANI−PAAMPSA's secondary couple are shown across pH 3−6 for comparison. The solid line represents a linear fit of $E_{1/2}$ from pH 3−7, yielding a slope of −111.8 mV/decade. The dashed line represents a linear fit of $E_{1/2}$ from pH 8 to 10, yielding a slope of −71.1 mV/decade.

To determine the dependence of the redox couples of PANI−PAAMPSA on proton concentration, we acquired CVs on PANI−PAAMPSA across a pH range of 3−10. Individual CVs as a function of pH are shown in Figure 2. Below pH 7, the CVs of PANI−PAAMPSA are characteristically similar to that shown in Figure 1. With increasing pH, the primary couple shifts to higher potentials while the secondary couple is largely pH independent. Above pH 7, however, the CVs of PANI−PAAMPSA only exhibit a single redox couple that shifts moderately with increasing alkalinity. There therefore appears to be two distinct pH regimes in which the redox behavior of PANI−PAAMPSA is characteristically different.

To quantitatively assess the redox behavior of PANI−PAAMPSA in these two regimes we extracted and plotted the redox potentials associated with the primary and secondary couples below pH 7 and those associated with the single couple above pH 7 in Figure 3. For pH 3−9 these potentials represent the average of two measurements on a single PANI−PAAMPSA modified glassy-carbon electrode, one determined with increasing pH (shown in Figure 2) and the other with decreasing pH; error bars indicate the standard deviations of 10 cycles in each direction. The redox potentials at pH 10 were derived from a fresh electrode due to diminished electroactivity accompanying prolonged immersion in buffer solutions. Examining the pH dependence of the primary couple across pH 3−7 and that of the single couple beyond pH 7 we notice that the reduction potential (E_{red}) exhibits a steeper pH dependence at basic conditions compared to that at acidic or neutral conditions as the solution struggles to provide the necessary protons to accommodate reduction of PANI−PAAMPSA at pH > 7. Conversely, the oxidation potential (E_{ox}) exhibits higher sensitivity at acidic conditions. The secondary redox potentials, extracted from the CV scans in the pH range of 3−7, do not display any variation with proton concentration.

Given the E_{red} and E_{ox}, we calculated $E_{1/2}$, where $E_{1/2} = 1/2(E_{red} + E_{ox})$; $E_{1/2}$ values are also plotted in Figure 3 as a function of pH. A linear fit of $E_{1/2}$ of the primary couple yields a slope of −111.8 mV/decade across pH 3−7 and is consistent with a 2 proton per electron redox process, suggesting that the primary redox couple observed in the range of pH 3−7 is associated with the PB/ES transition and not the PB/EB transition. Consistent with this assignment, the secondary redox couple is pH independent. The secondary couple can thus be attributed to an ES/LB transition where there is no proton transfer during this redox process. A similar fit to $E_{1/2}$ at higher pH reveals a slope of −71.1 mV/decade and is more consistent with a 1 proton per electron redox process. We thus attribute the single redox couple observed in the CVs at pH 8−10 to a direct PB/LB transition. These values deviate slightly from the ideal pH dependence of the redox potential predicted by eq 1. Specifically, for a two proton per electron redox process, eq 1 predicts a potential change of −118 mV/decade pH, whereas for a single proton per electron process, eq 1 predicts −59 mV/decade pH. We speculate that our extracted slope from the primary redox couple of the CVs acquired at pH 3−7 is sub-118 mV/decade because of mass-transfer limitations of the protons. Specifically, the polymer acid matrix hinders diffusion of protons when PANI−PAAMPSA is oxidized from ES to PB; that free protons are confined locally eases their subsequent reincorporation upon reduction back to ES. Indeed, this phenomenon is not unique to the CVs of PANI−PAAMPSA but more commonly observed in the CVs of polymer acid doped PANI systems. For example, the repeated cycling of poly(acrylic acid) doped PANI with potential yields a pH dependence of −110 mV/decade across pH 0.0−4.0,[38] whereas well-documented studies of small-molecule acid doped PANI yield $E_{1/2}$ dependencies of the primary couple of −120 mV/decade, more inline with what the Nernst equation predicts, in the pH range from −0.20 to 4.0.[39] On the other hand, we observe a steeper than expected slope in the range of pH 8−10. We believe this observation stems from proton deficiencies in the alkaline environment and attribute the excess potential to the overpotential necessary to strip protons from the alkaline buffer solution.

The electroactivity of PANI−PAAMPSA persists through pH 10.2, surpassing the electroactive range of small-molecule acid doped PANI by nearly 5 decades[40,41] and that of previously reported polymer acid doped PANI by 3 decades.[42] While we currently do not know how template-

(38) Cai, L. T.; Chen, H. Y. *J. Appl. Electrochem.* **1998**, *28*, 161.
(39) Huang, W.-S.; Humphrey, B. D.; MacDiarmid, A. G. *J. Chem. Soc., Faraday Trans. 1* **1986**, *82*, 2385.
(40) Diaz, A. F.; Logan, J. A. *J. Electroanal. Chem.* **1980**, *111*, 111.
(41) Yue, J.; Epstein, A. J.; Macdiarmid, A. G. *Mol. Cryst. Liq. Cryst.* **1990**, *189*, 255.
(42) Ge, C.; Armstrong, N. R.; Saavedra, S. S. *Anal. Chem.* **2007**, *79*, 1401.

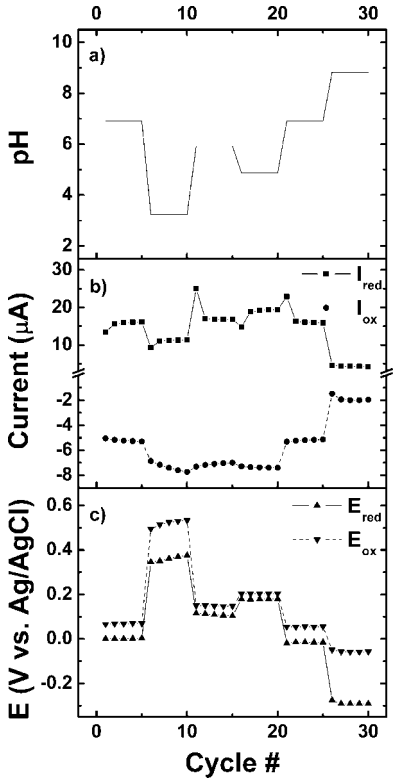

Figure 4. Oxidation and reduction behavior of PANI−PAAMPSA on a glassy-carbon electrode as a function of consecutive cycle no. and pH. The scan rate was held constant at 20 $mV \cdot s^{-1}$ for 5 cycles. (a) Randomized buffer pH associated with each cycle set. (b) Variations in oxidation (●) and reduction (■) current upon extended cycling. (c) Corresponding redox potentials (▼ and ▲, respectively).

polymerized PANI−PAAMPSA maintains electroactivity across such a broad pH range, we speculate the specific interactions between the aniline mers and PAAMPSA affords a structural stability that is absent in other polymer acid doped systems. Early studies with poly(styrene sulfonic acid) doped PANI showed enhanced pH stability near pH 4 relative to styrene sulfonic acid doped PANI.[23] The material's redox behavior, however, was not investigated at elevated pH. Across pH 0−4 its electroactivity showed a weaker pH dependence compared to our PANI−PAAMPSA. It seems that the ionic interactions rendered by the sulfonic acid groups in both of these polymer acids are not solely responsible for the stability of PANI's electrochemical response; the additional amide groups on PAAMPSA, capable of hydrogen bonding, must provide a contributing role as well. Structural studies are currently underway to identify the nature of PANI and PAAMPSA's unique relationship.

Reversibility of Electrochemical Response and Stability of Electroactivity. PANI−PAAMPSA films were subjected to repeated potential cycling to highlight the reversibility of its electrochemical environment with applied potential. Figure 4 shows a panel graph illustrating the film's electrochemical response to a variety of pH conditions. A single PANI−PAAMPSA-coated glassy-carbon electrode was subject to a 5-cycle CV experiment in a random sequence of buffers of equal strength but varying pH, as shown in Figure 4a. Each set of cycles lasted 650 s, after which the electrode was soaked in deionized water for ∼1 min before immersing in the next buffer solution of a different pH.

Figure 4b shows the current response of the primary oxidation (I_{ox}) and reduction (I_{red}) peaks as a function of cycle number. I_{ox} increases and decreases congruent with pH. I_{red} generally trends with pH as well; we observe slight deviations in a near-neutral pH of 5−7 as the primary reduction peak broadens. More importantly, the modulation in I_{ox} and I_{red} is very stable with respect to pH; returning PANI−PAAMPSA to pH 7 after exposure to pH 3, 6, and 5 results in the same current levels previously measured at pH 7. Though highly sensitive to pH, PANI−PAAMPSA thus exhibits a large degree of reversibility. This reversibility strongly dismisses any question of degradation. The sixth and final set of cycles was measured at pH 9; comparison with the CVs shown in Figure 2 shows that the peak current levels match the expected values. We notice, however, transient effects in I_{red} where the initial current upon switching pH is different from that extracted from subsequent cycles. Specifically, we observe an overshoot in I_{red} when switching to a higher pH and an undershoot when switching to a lower pH. We speculate that this transient effect is a result of an initial efflux of protons from the PANI−PAAMPSA-modified electrode upon immersion in a more basic solution, positively contributing to the measured current. Upon immersion in a more acidic solution, however, a transient influx of protons would conversely occur and mitigate the measured response. It should be noted that the experiments summarized in Figure 4 were initiated at the oxidizing extreme (0.9 V vs Ag/AgCl), so the cycles start with a reducing sweep. When the CV experiments start at the reducing extreme so the cycle begins with an oxidizing sweep (not shown), transient undershoots and overshoots are observed in I_{ox} instead of I_{red}.

Figure 4c shows the potential response of the primary oxidation (E_{ox}) and reduction (E_{red}) peaks as a function of cycle number. The potential response tracks changes in pH systematically, again confirming the stability and reversibility of PANI−PAAMPSA. The potential response, however, does not exhibit the transient effects observed in the current response. Unlike the current response, which closely corresponds to the amount of material reacting, the peak potentials are indicative of the chemical species that are present and therefore less vulnerable to transient effects due to changes in pH. Furthermore, the peak potentials obtained on random cycling of pH are comparable with those obtained on systematic increase in pH (Figure 3), which resolutely illustrates the robust nature of PANI−PAAMPSA's electroactivity. The sensitivity and stability of the material's redox properties toward pH over a range of 3−9 coupled with the ease of film preparation suggest PANI−PAAMPSA as a promising candidate for pH monitoring and analyte sensing.

Spectroelectrochemical Clarification of Oxidation and Dopant States. Although EB and ES are not directly distinguishable electrochemically, spectral characterization in the UV−vis/NIR range can easily distinguish between the two. Representative UV−vis/NIR spectra for the four forms of PANI (LB, EB, ES, and PB) are shown in Figure 5. PANI's oxidation and protonation state can be tracked by

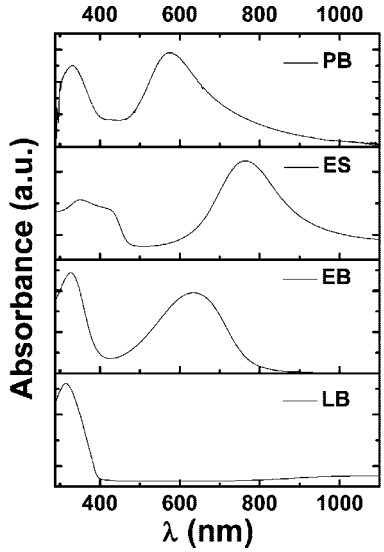

Figure 5. Representative UV−vis/NIR spectra of LB, EB, ES, and PB forms of PANI−PAAMPSA.

following three spectral characteristics: $\lambda = 320$, 420, and 700 nm, colloquially termed the benzenoid, polaronic shoulder, and polaron regions, respectively. Synchronous correlation spectroscopy analyses,[43,44] included in the Supporting Information, have identified these regions as the most dynamic during electrochemically induced transitions.

The region near 320 nm serves as a probe of the benzenoid moiety and can be used to identify LB.[45] Upon reduction to LB, this region of the UV−vis spectrum experiences significant growth at the expense of the polaron and the polaronic shoulder, both of which are simultaneously suppressed to negligible levels. The shoulder near 420 nm is uniquely related to the ES form of PANI and should be absent in all other states.[46] Broad absorption peaks in the region of 500−900 nm are observed in EB, ES, and PB, though at different locations. When this peak is centered at <600 nm wavelengths, PB is the dominant state;[47] when centered near 650 nm, the dominant form is EB.[48] When centered near 800 nm, however, ES is the dominant state[49] and the peak often exhibits a free carrier tail that extends into the NIR for highly conductive samples.[50]

Spectroelectrochemistry provides further proof that ES, rather than EB, is PANI−PAAMPSA's preferred state in between the PB and LB extremes, even in weakly acidic conditions. The panel graph in Figure 6 shows a cyclic voltammogram at pH 5 (a) and $\partial/\partial E$ Abs(λ) where $\lambda = 320$ (b), 420 (c), and 700 nm (d) during the same cycle. Given Beer's Law, we can qualitatively comment on the changes

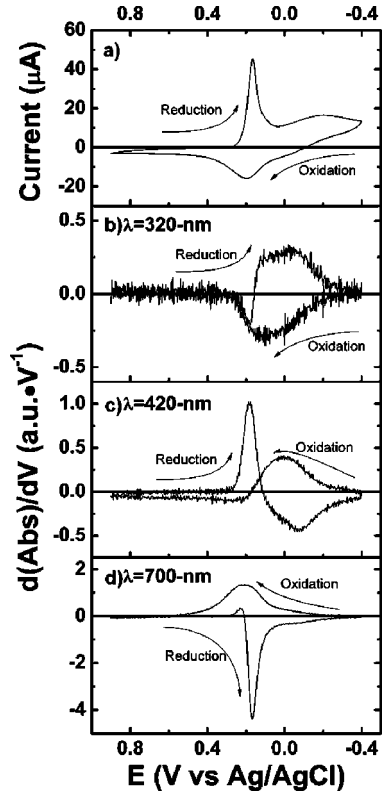

Figure 6. Electrochemical and electrochromic response of PANI−PAAMPSA spun on bisphosphonic acid modified ITO at 5000 rpm to potential cycling at 1 mV•s^{-1} in 100 mM pH 5.0 acetate buffer solution: (a) Cyclic voltammogram of film shows primary and secondary couples consistent with Figure 1. (b, c, and d) Changes in absorbance at $\lambda = 320$, 420, and 700 nm (corresponding to the benzenoid peak, polaronic shoulder, and polaron, respectively) with respect to potential as a function of potential.

in the concentrations of the species present by tracking the derivatives of the absorbances of these spectral characteristics during cycling.

Figure 6a shows the third CV cycle of PANI−PAAMPSA spun on bisphosphonic acid modified ITO and measured in 100 mM pH 5 acetate buffer solution at 1 mV•s^{-1}. In the absence of bisphosphonic acid treatment, PANI−PAAMPSA delaminates almost immediately upon immersion in buffer solution. With bisphosphonic acid treatment, PANI−PAAMPSA maintains its structural, mechanical, and electrochemical integrity during continuous immersion in buffer solution throughout the 130 min experiment. Comparison with the CV shown in Figure 1, performed on a glassy-carbon electrode, shows a 70 mV shift in the primary redox couple toward reducing potentials but otherwise maintains identical peak shapes and separations. The lack of any additional peaks in the CV further confirms that the bisphosphonic acid modification performed on the electrode is electrochemically inert.

Figure 6b shows changes of the UV−vis absorbance at 320 nm with respect to applied potential. Since the absorbance is directly proportional to concentration, tracking the first derivative (with respect to potential) of the absorbance at 320 nm allows us to assess the concentration fluctuations in the benzenoid region. On reduction, we observe a sudden growth in absorbance beginning at 0.15 V. This potential coincides with the peak of the primary reduction reaction

(43) Noda, I.; Dowrey, A. E.; Marcott, C.; Story, G. M.; Ozaki, Y. *Appl. Spectrosc.* **2000**, *54*, 236A.
(44) Noda, I. *Appl. Spectrosc.* **1993**, *47*, 1329.
(45) Stilwell, D. E.; Park, S.-M. *J. Electrochem. Soc.* **1989**, *136*, 427.
(46) McManus, P. M.; Yang, S. C.; Cushman, R. J. *J. Chem. Soc., Chem. Commun.* **1985**, *22*, 1556.
(47) Sun, Y.; MacDiarmid, A. G.; Epstein, A. J. *J. Chem. Soc., Chem. Commun.* **1990**, *7*, 529.
(48) Stafström, S.; Brédas, J. L.; Epstein, A. J.; Woo, H. S.; Tanner, D. B.; Huang, W. S.; MacDiarmid, A. G. *Phys. Rev. Lett.* **1987**, *59*, 1464.
(49) Ginder, J. M.; Epstein, A. J. *Phys. Rev. B: Condens. Matter* **1990**, *41*, 10674.
(50) McManus, P. M.; Cushman, R. J.; Yang, S. C. *J. Phys. Chem.* **1987**, *91*, 744.

shown in Figure 6a. The absorbance associated with the benzenoid peak continues to grow, albeit at a slower pace, across the entire range of reducing potentials; this observation is consistent with the increase in benzenoid concentration as ES is reduced to LB. The benzenoid region begins to decay immediately after reversal of the applied potential. The rate of decay peaks near 0.1 V but continues until 0.3 V and remains static for the remainder of the sweep. This potential range coincides with completion of the CV's secondary oxidation reaction and is consistent with the decrease in benzenoid concentration as LB is oxidized to ES.

Figure 6c shows changes in absorbance at 420 nm with respect to potential. A sharp growth in the absorbance associated with the polaronic shoulder occurs near 0.30 V. This growth directly corresponds to the onset of the primary reduction peak shown in Figure 6a and provides clear evidence that PB reduces to ES (and not EB). Decay in the 420 nm absorbance band begins soon after, however, concurrent with the broad ES to LB reduction indicated in the CV in Figure 6a. Growth of the absorbance associated with the polaronic shoulder in the UV−vis spectrum resumes upon potential reversal, peaking at 0.0 V and continuing until 0.18 V. This potential window falls between the two oxidation peaks and confirms ES as the product of LB oxidation.

Figure 6d shows changes in the absorbance at 700 nm with respect to potential and reflects fluctuations in the polaron region. The reduction sweep results in temporary growth of the absorbance of the polaron peak in the UV−vis spectrum between 0.3 and 0.2 V followed by a sudden decay until 0.0 V. This shift corresponds to the primary reduction reaction; it reflects the decline in the absorbance of the PB polaron at 550 nm and simultaneous emergence and growth of the ES polaron at 700 nm and then toward 800 nm. Decay of the polaron absorbance continues through the remainder of the reduction sweep but at a negligible rate. During the oxidation sweep, growth of the polaron absorbance at 700 nm does not become significant until 0.1 V. This potential corresponds to the onset of the primary oxidation reaction. During oxidization from ES to PB the polaron growth exhibits a peak breadth comparable to that of the voltammogram's primary oxidation peak. The similarity between the polaron growth and the CV shown in Figure 6a emphasizes the coupled nature of spectral and electrochemical characterization. PB $\leftrightarrow$ ES $\leftrightarrow$ LB transitions are reversible and observed during repeated potential cycling in buffer solutions with pH $\leq$ 7. In more alkaline buffer solutions, spectroelectrochemical experiments confirm a direct PB to LB transition that is consistent with the observation of a single redox couple in CV experiments. For completeness, the spectroelectrochemical data acquired at pH 9 are provided in the Supporting Information. Cumulatively, these results strongly support the supposition suggested by our pH studies: in acidic conditions ES is the product of PB reduction and LB oxidation, exhibiting remarkable stability even at pH 7.0; at alkaline conditions, ES is not isolatable and direct PB/LB transitions dominate. The PB/LB transition remains highly reversible.

Conclusion

We have shown the conductive form of water-dispersible polymer acid doped PANI to persist though pH 7 and electroactivity persisting in excess of pH 10. Due to the ease with which PANI−PAAMPSA is produced and processed, the unique nature of its 3 oxidation states + doped form, and significant electroactivity at and beyond physiological pH, a thorough understanding of its redox capabilities could help usher in commercial applications. A current investigation of the use of polymer electronics in brain-monitoring electrodes has found PANI−PAAMPSA to exhibit biocompatibility toward both *E. coli* and mammalian fibroblast cells.[51] Finding new methods of controlling its properties electrochemically are promising routes toward harnessing the wide range of potential uses of PANI.

Acknowledgment. This work was supported by the Beckman Young Investigator Award. J.D.T. acknowledges funding from an NSF Graduate Fellowship. The authors also thank Dr. Adam Heller for useful discussions and instruction in the initial stages of this project.

Supporting Information Available: Synchronous correlation spectroscopy of PANI-PAAMPSA's spectroelectrochemistry at pH 5, electrochemical and electrochromic response of PANI-PAAMPSA at pH 9.0. This material is available free of charge via the Internet at http://pubs.acs.org.

CM802314H

(51) Collier, K. A. Senior Thesis, Princeton University, 2008.